International Journal of Engineering Science 182 (2023) 103770

Contents lists available at ScienceDirect

International Journal of Engineering Science

journal homepage: www.elsevier.com/locate/ijengsci

A multiphysics model for the thermoelectric dissociation of gas hydrates

T.I. Zohdi [a],[*], G.J. Moridis [b]

[a] Department of Mechanical Engineering, UC Berkeley, United States of America
[b] Department of Petroleum Engineering, Texas A & M University, United States of America

ARTICLE INFO

Keywords:
Gas hydrates
Multiphysics
Model
Simulation

ABSTRACT

This work develops a model and rapid simulation strategy for the electrically-driven dissociation (unlocking) of subsurface gas hydrates. There are two schools of thought, as to how electrical fields can dissociate gas hydrates:

Case 1: gas hydrates are dissociated (unlocked) by an appropriate intensity and frequency of the electric field,

Case 2: gas hydrates are dissociated by an appropriate level of Joule heating.

In either case, one must resolve the thermoelectric fields within a heterogeneous medium consisting of encapsulated gas hydrates in a interstitial material. Accordingly, the objective of this work is to develop an easy-to-calibrate model and rapid simulation strategy to guide the delivery of an appropriate current and electrical field, as well as an appropriate level of Joule heating. The approach utilizes a coupled system of equations based on: (1) an electrical-flow submodel, (2) a thermal field evolution submodel, (3) a thermoelectric and frequency-dependent attenuation and (4) a spatio-temporal Finite-Difference Time Domain (FDTD) discretization of the coupled field equations. The model can be rapidly computed and allows analysts to vary parameters quickly, which facilitates the potential use of Machine Learning paradigms for data-model calibration. Numerical studies are provided to illustrate the behavior of the model.

1. Introduction

Gas hydrates are solid crystalline compounds in which gas molecules are encased inside the lattices of ice crystals. These gases are referred to as *guests*, whereas the ice crystals are called *hosts*. Of particular interest are hydrates in which the gas is a hydrocarbon. For in depth discussions on the physics of gas hydrates, the reader is referred to the following: Aleksandrof, Dzhuraeva, and Utenkov (2013), Anno, Moridis, and Blasingame (2021) Atkinson (2002), Ballard (2002), Bear (1972), Bird, Stewart, and Lightfoot (2007), Chung, Ajlan, Lee, and Starling (1988), Driesner (2007), Driesner and Heinrich (2007), Hass (1976), IAPWS1-8 International Association for the Properties of Water and Steam (IAPWS) (1997, 2007, 2008, 2009, 2011a, 2011b, 2012), International Formulation Committee (1967), Kim, Bishnoi, Heideman, and Rizvi (1987), Klinkenberg, Mao and Duan (2009), Millington and Quirk (1961), Moridis (2014), Moridis and Pruess (2014), Peng and Robinson (1976), Pruess, Oldenburg, and Moridis (1999) and Pruess, Oldenburg, and Moridis (2012).

---

[*] Corresponding author.
E-mail addresses: zohdi@berkeley.edu (T.I. Zohdi), moridis@tamu.edu (G.J. Moridis).

https://doi.org/10.1016/j.ijengsci.2022.103770
Received 14 September 2022; Accepted 10 October 2022

1.1. Gas hydrates and their potential

Gas hydrates are solid crystalline compounds in which gas molecules (guests) occupy the lattices of ice-like solid crystal structures (hosts). Gas hydrates look and behave like ice, but they contain large amounts of methane. They are known to occur on every continent and exist in tremendous quantities in marine sediments layers that are several hundred meters thick directly below the sea floor and in the permafrost in the Arctic. *The potential for gas hydrates as an energy source is staggering.* In this work, our primary interest is in extracting natural gas by thermoelectrically dissociating gas hydrates. However, for this process to be successful, it requires modeling and simulation tools. Gas hydrates were first discovered in laboratory studies around 1800. However, it was only until approximately 1965 that mankind first recognized that they are widespread in nature (Sloan & Koh, 2008). Although there has been no systematic effort to map and evaluate this resource, current estimates are that the Earth's crust hold betweens *500 to 2,500 Gigatons*. Thus, methane hydrates potentially provide a gigantic unconventional energy source, which is also cleaner burning than coal or oil (see Klauda & Sandler, 2005; Milkov, 2004 and Sloan & Koh, 2008). Given the potential magnitude of this resource, the ever-increasing global energy demand, and finite conventional fossil fuel reserves, the potential of gas hydrates as an energy source demands technical and economic evaluation. A thorough discussion of the global distribution of the hydrate resource, a synopsis of global research activities, identification of production targets and methods to predict and analyze production from natural accumulations, as well as on a wide range of issues associated with such production, can be found in the review articles of Moridis, Collett, Boswell, Kurihara, Reagan, Koh, and Sloan (2009), Moridis, Collett, Pooladi-Darvish, Hancock, Santamarina, Boswell, Kneafsey, Rutqvist, Kowalsky, Reagan, Sloan, Sum, and Koh (2011), Boswell, Hancock, Yamamoto, Collett, Pratap, and Lee (2020) and Kastner, Myers, Koh, Moridis, Johnson, and Thurmond (2022).

1.2. Hydrate dissociation by electromagnetic (EM) fields

The effects of externally applied electric and electromagnetic (EM) fields to extract gas hydrates is technologically challenging (English & MacElroy, 2015), and has received sporadic attention. Makogon (1997) was the first to investigate electric-field effects on CH4-hydrates and to develop thermodynamic-equilibrium expressions relating the effect of time-variable EM fields to hydrate stability. The first patent on the US of EM fields to prevent hydrate formation in pipelines was awarded to Rojey (1997) and was based on theoretical concepts without any supporting computational and experimental confirmatory work. It asserted that EM waves of particular intensity and frequency ranges can disrupt the molecular organization in hydrates, causing their dissociation. There are two schools of thought on how electrical fields can dissociate gas hydrates: (1) gas hydrates are dissociated by the appropriate intensity and frequency of the electric field or (2) gas hydrates are dissociated by the appropriate level of Joule heating. Of course, a combination of effects could also be possible. In either case, one must resolve the thermoelectric fields within a heterogeneous medium consisting of encapsulated gas hydrates in an interstitial medium. Accordingly, the present work develops a computational model for electrically-driven dissociation. The present model develops a coupled system of equations based on (1) an electrical-flow submodel and (b) a thermal field evolution submodel, with embedded thermoelectric and frequency-dependent attenuation. A spatio-temporal Finite-Difference Time Domain (FDTD) discretization of the coupled field equations is also developed, which can be rapidly simulated, thus enabling analysts to explore large parameter ranges quickly. This facilitates the potential use of Machine Learning paradigms for data calibration, inverse problem calculations and optimization. Numerical studies are provided to illustrate the behavior of the model.

2. Governing equations

We consider a model problem (Fig. 1), which is in the form of a one-dimensional long cylinder (a core sample) with an applied oscillatory current at the top. There are two coupled field equations that need to be solved. Later, a Finite Difference grid will be used to solve the resulting differential equations.

2.1. Macroscale electrical current flow

The conservation of current (assuming that the electrical flow is virtually instantaneous-not time-transient, relative to the evolution the of temperature) is derived by taking a control volume shown in Fig. 2

$$+(J)^{-}-(J)^{+}-\mathcal{L}^{J}\Delta z=0, \tag{1}$$

where J is the current and $\mathcal{L}$ is the loss per unit length. Assigning $J^{-}=J(z)$ and $J^{+}=J(z)+\Delta J$, and as $\Delta z\rightarrow 0$, we obtain

$$\frac{\partial J}{\partial z}=-\mathcal{L}^{J}. \tag{2}$$

Making the standard assumption that the losses correlate to the intensity of the current, we have:

$$\frac{\partial J}{\partial z}=-\mathcal{L}^{J}=-aJ\Rightarrow\frac{dJ}{J}=-a\,dz\Rightarrow J(z)=Ce^{-\int_{0}^{z}a\,dz}, \tag{3}$$

where a is the loss coefficient. Applying the oscillatory boundary condition $J(z=0)=J_{o}sin\frac{2\pi\omega t}{T}$ yields

$$J(z)=J_{o}sin\frac{2\pi\omega t}{T}e^{-\int_{0}^{z}a\,dz}. \tag{4}$$

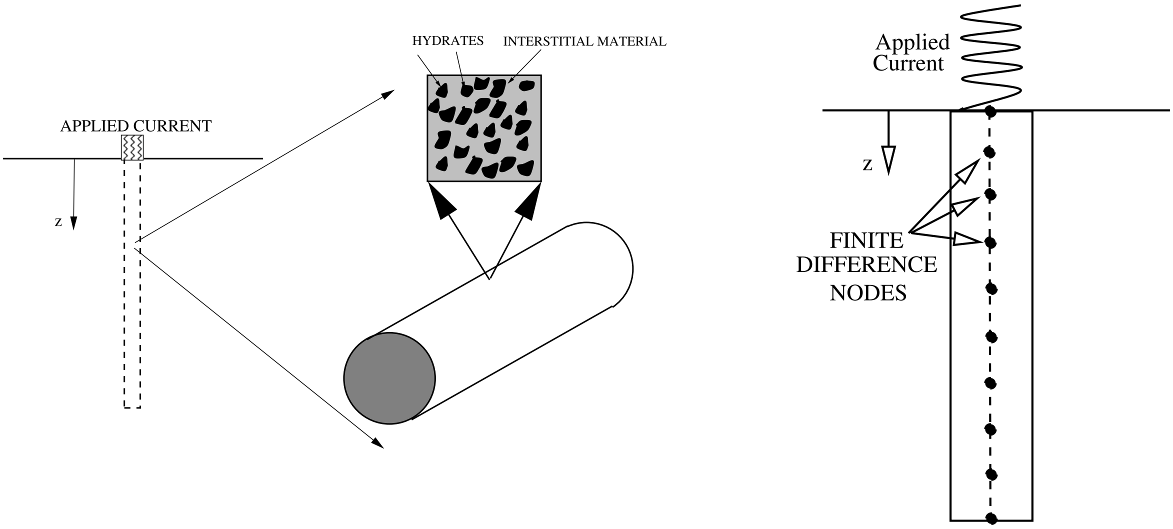

Fig. 1. The set up of the model problem consisting of a core sample with heterogeneous material microstructure with an applied electrical current.

Assuming $a \neq a(z)$ yields

$$J(z) = J_o sin\frac{2\pi\omega t}{T}e^{-az}, \tag{5}$$

which is a Beer–Lambert type equation for electrical attenuation. To obtain the electric field (E), one uses Ohm's Law:

$$J = \sigma^c E \Rightarrow E(z) = \frac{1}{\sigma^c(z)}J_o sin\frac{2\pi\omega t}{T}e^{-az}, \tag{6}$$

where σ^c is the electrical conductivity, ω is the applied frequency, T is the time period and t is the time. The product of J and E produces Joule heating

$$H(z) = JE = \frac{J^2}{\sigma^c} = \frac{1}{\sigma^c(z)}(J_o sin\frac{2\pi\omega t}{T}e^{-az})^2. \tag{7}$$

Remarks. In the regimes of interest, the attenuation of electromagnetic radiation grows with frequency (inversely proportional to wavelength). A simple relation is

$$a(\omega) = a_o e^{a_1\omega}, \tag{8}$$

where a_o is a baseline value and a_1 is a growth coefficient.[1] The electrical conductivity also has a thermal field dependency, for example

$$\sigma^c(\theta) = \sigma^c_o e^{-a_2\frac{\theta-\theta^o}{\theta^o}}, \tag{9}$$

where a_2 is a thermal decay parameter for the electrical conductivity and θ_o is a reference temperature. Finally, we note that the flow of current could be reformulated in terms of the voltage, $V = -\frac{\partial E}{\partial z}$ to read

$$\frac{\partial J}{\partial z} = \frac{\partial(\sigma^c E)}{\partial z} = -\frac{\partial}{\partial z}(\sigma\frac{\partial V}{\partial z}) = 0, \tag{10}$$

where the voltage is controlled at the ends $V(z = 0) = V_o$ and $V(z = L) = V_L$, although this is unnecessary for this present formulation.

2.2. Macroscale temperature evolution

The heat equation (a simplified version of the First Law of Thermodynamics) reads as follows for a control volume

$$\rho C\frac{\partial\theta}{\partial t} = \frac{\partial}{\partial z}(\mathbb{K}\frac{\partial\theta}{\partial z}) + \alpha JE - \mathcal{L}^\theta, \tag{11}$$

---

[1] Attenuation coefficients have a general trend of growth with increase of wavelength (inducing an increase in attenuation). In the regimes of interest, the attenuation of electromagnetic radiation grows with frequency (inversely proportional to wavelength). The relation chosen reflects that basic trend. To the knowledge of the authors, for gas-hydrate media, there is no general formula. Of course, experiments combined with Machine Learning enable calibration, can yield such a relation.

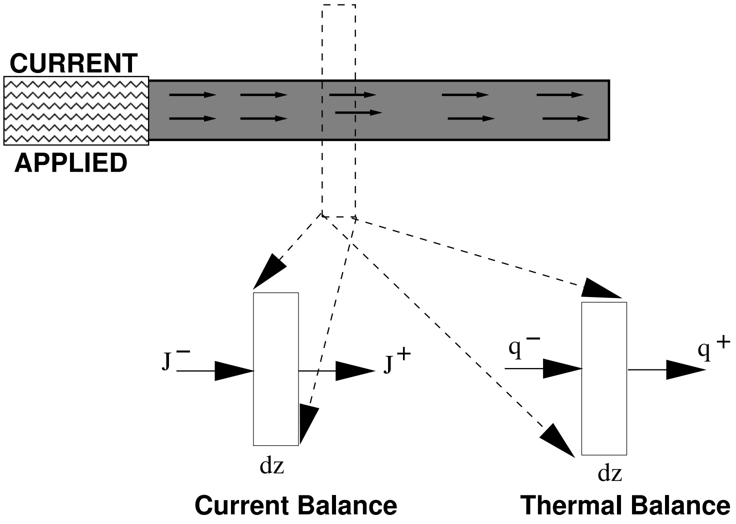

Fig. 2. The flow of the current through a core material sample.

where $0 \leq \alpha \leq 1$ is the heating efficiency, $\mathbb{K}$ is the thermal conductivity, ρ is the mass density, C is the heat capacity and where the thermal losses to the surroundings are

$$\mathcal{L}^{\theta} \approx \beta(\theta(z,t) - \theta^{surr}), \tag{12}$$

where β is a loss parameter and θ^{surr} is the surrounding environment, which leads to

$$\frac{\partial \theta}{\partial t} = \frac{1}{\rho C}\frac{\partial}{\partial z}\left(\mathbb{K}\frac{\partial \theta}{\partial z}\right) + \frac{\alpha J E}{\rho C} - \beta\frac{(\theta(z,t) - \theta^{surr})}{\rho C}. \tag{13}$$

For compactness, we define the righthand side in the following manner

$$\frac{1}{\rho C}\left(\frac{\partial}{\partial z}\left(\mathbb{K}\frac{\partial \theta}{\partial z}\right) + \alpha J E - \beta(\theta(z,t) - \theta^{surr})\right) \overset{\text{def}}{=} \mathcal{F}(z,t) \tag{14}$$

3. Numerical approximations

In order to solve the thermal evolution equation, we employ a spatio-temporal Finite-Difference Time Domain discretization of the field equations (Fig. 1). We approximate the time derivative of $\theta(z)$ at z and t as

$$\frac{\partial \theta}{\partial t} \approx \frac{\theta(z, t + \Delta t) - \theta(z,t)}{\Delta t}, \tag{15}$$

where, for the derivative term inside of $\mathcal{F}$, we approximate the spatial derivatives in heat conduction with a second order scheme:

$$\frac{\partial q}{\partial z}|_z \approx \frac{q(z + \frac{\Delta z}{2}) - q(z - \frac{\Delta z}{2})}{\Delta z}, \tag{16}$$

where (in conjunction with Fourier's Law)

$$q(z + \frac{\Delta z}{2}) \approx -\mathbb{K}(z + \frac{\Delta z}{2})\underbrace{\frac{\theta(z + \Delta z) - \theta(z)}{\Delta z}}_{\frac{\partial \theta}{\partial z}|_{z+\frac{\Delta z}{2}}} \tag{17}$$

and

$$q(z - \frac{\Delta z}{2}) \approx -\mathbb{K}(z - \frac{\Delta z}{2})\underbrace{\frac{\theta(z) - \theta(z - \Delta z)}{\Delta z}}_{\frac{\partial \theta}{\partial z}|_{z-\frac{\Delta z}{2}}}, \tag{18}$$

where

$$\mathbb{K}(z + \frac{\Delta z}{2}) \approx \frac{1}{2}(\mathbb{K}(z + \Delta z) + \mathbb{K}(z)), \tag{19}$$

and

$$\mathbb{K}(z - \frac{\Delta z}{2}) \approx \frac{1}{2}(\mathbb{K}(z) + \mathbb{K}(z - \Delta z)). \tag{20}$$

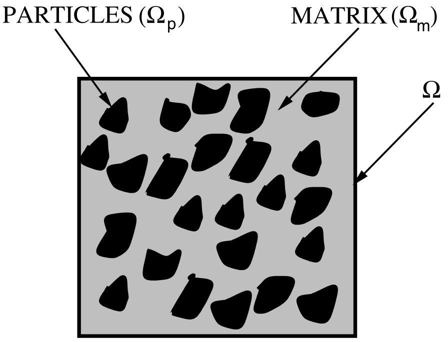

Fig. 3. A Representative Volume Element (RVE).

This is computed at each node in the grid, leading to the following formula:

$$\theta(z,t+\Delta t)=\theta(z,t)+\Delta t\mathcal{F}(z,t). \tag{21}$$

4. Microscale–macroscale analysis for heterogeneous media

Thus far, the properties appearing in the previous macroscale analysis of the core sample are *effective properties*. We will consider the analysis of two main transport properties: (1) the effective electrical conductivity and (2) the effective thermal conductivity.

4.1. Effective electrical conductivity

A primary property of interest is the overall "effective" macroscale electrical conductivity, defined via volume averages posed over a statistically representative volume element with domain Ω (Fig. 3)

$$\langle \boldsymbol{J}\rangle_\Omega=\boldsymbol{\sigma}^{c,*}\cdot\langle \boldsymbol{E}\rangle_\Omega, \tag{22}$$

where

$$\langle\cdot\rangle_\Omega\overset{\text{def}}{=}\frac{1}{|\Omega|}\int_\Omega\cdot\,d\Omega, \tag{23}$$

and where $\boldsymbol{\sigma}^{c,*}$ is the effective conductivity for the mixture, $\langle \boldsymbol{E}\rangle_\Omega$ is the volume averaged electric field, $\langle \boldsymbol{J}\rangle_\Omega$ is the volume averaged current and where the averaging operator is defined as $\langle\cdot\rangle_\Omega\overset{\text{def}}{=}\frac{1}{|\Omega|}\int_\Omega(\cdot)\,d\Omega$. When the materials are isotropic, $\boldsymbol{\sigma}^{c,*}=\sigma^{c,*}\mathbf{1}$.

4.2. Effective thermal conductivity

The other key transport property is overall thermal conductivity:

$$\langle \boldsymbol{q}\rangle_\Omega=-\boldsymbol{I\!K}^*\cdot\langle\nabla\theta\rangle_\Omega, \tag{24}$$

where $\boldsymbol{I\!K}^*$ is the effective thermal conductivity for the mixture, ($\boldsymbol{I\!K}^*=I\!K^*\mathbf{1}$ when isotropic), $\langle \boldsymbol{q}\rangle_\Omega$ is the volume averaged thermal flux field, $\langle\nabla\theta\rangle_\Omega$ is the volume averaged thermal gradient field flux.

4.3. Macroscale conductivity estimates

In order to make estimates of the overall properties of a mixture, we consider the widely used Hashin and Shtrikman bounds for isotropic materials with isotropic effective responses (Hashin and Shtrikman (1962a), Hashin and Shtrikman (1963) and Hashin and Shtrikman (1962b)). These estimates provide one with upper and lower bounds on the overall response of the material. For two isotropic materials with an overall isotropic response we utilize the following estimates.

$$\underbrace{\sigma_1^c+\frac{v_2^c}{\frac{1}{\sigma_2^c-\sigma_1^c}+\frac{1-v_2^c}{3\sigma_1^c}}}_{\sigma^{c,*,-}}\leq\sigma^{c,*}\leq\underbrace{\sigma_2^c+\frac{1-v_2^c}{\frac{1}{\sigma_1^c-\sigma_2^c}+\frac{v_2^c}{3\sigma_2^c}}}_{\sigma^{c,*,+}}, \tag{25}$$

where the conductivity of phase 2 (with volume fraction v_2^c) is larger than phase 1 ($\sigma_2^c\geq\sigma_1^c$). Usually, v_2^c corresponds to the particle material, although there can be applications where the matrix is more conductive that the particles. In that case, v_2^c would correspond to the matrix material. Provided that the volume fractions and constituent conductivities are the only known information about the microstructure, the expressions are the tightest bounds for the overall isotropic effective responses for two phase media, where the

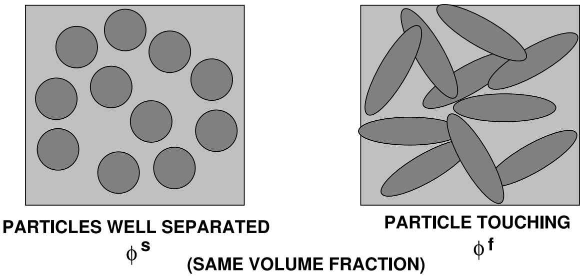

Fig. 4. Comparing microstructures with the same volume fractions. Flakes have many more contact points, and thus need a higher value of ϕ^c.

constituents are both isotropic. A critical observation is that the lower bound is more accurate when the material is composed of high conductivity particles that are surrounded by a low conductivity matrix (denoted case 1) and the upper bound is more accurate for a high conductivity matrix surrounding low conductivity particles (denoted case 2). This can be explained by considering two cases of material combinations, one with 50% low conductivity material and 50% high conductivity material. A material with a continuous low conductivity (fine-scale powder) binder (50%) will isolate the high conductivity particles (50%), and the overall system will not conduct electricity well (this is case 1 and the lower bound is more accurate), while a material formed by a continuous high conductivity (fine-scale powder) binder (50%) surrounding low conductivity particles (50%, case 2) will, in an overall sense, conduct electricity better than case 1. Thus, case 2 is more closely approximated by the upper bound and case 1 is closer to the lower bound. Since the true effective property lies between the upper and lower bounds, one can construct the following approximation

$$\sigma^{c,*} \approx \phi^c \sigma^{c,*,+} + (1-\phi^c)\sigma^{c,*,-}, \tag{26}$$

where $0 \le \phi^c \le 1$. ϕ^c *is function of the microstructure, and must be calibrated (see Fig. 4)* .

As mentioned, for high conductivity spherical particles, at low volume fractions, for example under 15%, where the particles are not making contact, the lower bound is more accurate. Thus, one would pick $\phi^c = \phi^s \le 0.5$ to bias the estimate to the lower bound. However, if we take the same volume fraction of particles, but make the flat flakes, they will certainly touch, and produce high-conductivity pathways. Their overall conductivity will certainly be higher than those of sphere at the same volume fraction. Thus, one would pick $\phi^c = \phi^f > \phi^s$. One can calibrate ϕ^c by comparing it to different experiments, as seen in Zohdi, Monteiro, and Lamour (2002). Essentially, the more the particles contact, the more relevant the upper bound becomes. The general trends are (a) for cases where the upper bound is more accurate, $\phi^c > \frac{1}{2}$ and (b) for cases when the lower bound is more accurate, $\phi^c < \frac{1}{2}$. ϕ^c indicates the degree of interaction of the particulate constituents.

Remarks. The literature on such methods is vast, dating back to Maxwell (1867), Maxwell (1873) and Rayleigh (1892), to estimate the overall macroscopic properties of heterogeneous materials. For an authoritative review of (a) the general theory of random heterogeneous media see Torquato (2002b), (b) for more mathematical homogenization aspects see Jikov, Kozlov, and Olenik (1994), (c) for solid-mechanics inclined accounts of the subject see Hashin (1983), Kachanov (1986, 1993), Kachanov and Sevostianov (2005), Kachanov, Tsukrov, and Shafiro (1994), Mura (1993), Nemat-Nasser and Hori (1999), (d) for analyses of cracked conductive media see Sevostianov, Gorbatikh, and Kachanov (2001) and (e) for computational aspects see Ghosh (2011), Ghosh and Dimiduk (2011) and Zohdi and Wriggers (2005, 2008). Tighter estimates, including generalized N-phase bounds can be found in Torquato (2002b).[2]

4.4. *Concentration tensors and macro–micro fields*

One can decompose the electrical field carried by each phase in the material as follows

$$\langle \boldsymbol{E} \rangle_\Omega = \frac{1}{|\Omega|}(\int_{\Omega_1} \boldsymbol{E}\, d\Omega + \int_{\Omega_2} \boldsymbol{E}\, d\Omega) = v_1 \langle \boldsymbol{E} \rangle_{\Omega_1} + v_2 \langle \boldsymbol{E} \rangle_{\Omega_2} \tag{27}$$

and the current can be decomposed as

$$\langle \boldsymbol{J} \rangle_\Omega = \frac{1}{|\Omega|}(\int_{\Omega_1} \boldsymbol{J}\, d\Omega + \int_{\Omega_2} \boldsymbol{J}\, d\Omega) = v_1 \langle \boldsymbol{J} \rangle_{\Omega_1} + v_2 \langle \boldsymbol{J} \rangle_{\Omega_2}, \tag{28}$$

The effective conductivity, $\boldsymbol{\sigma}^{c,*}$, defined via[3]

$$\langle \boldsymbol{J} \rangle_\Omega = \boldsymbol{\sigma}^{c,*} \cdot \langle \boldsymbol{E} \rangle_\Omega, \tag{29}$$

---

[2] Such N-phase bounds go well beyond the simple Wiener (1910), $\left(\sum_{i=1}^{N} v_i^c \sigma_i^{c,-1}\right)^{-1} \le \sigma^{c,*} \le \sum_{i=1}^{N} v_i^c \sigma_i^c$.

[3] Implicitly, we assume that (a) the contact between the phases is perfect and (b) the ergodicity hypothesis is satisfied (see Kröner, 1972 or Torquato, 2002b).

can be re-written in the following manner

$$\begin{aligned}\langle \boldsymbol{J}\rangle_{\Omega} &= v_1^c\langle \boldsymbol{J}\rangle_{\Omega_1} + v_2^c\langle \boldsymbol{J}\rangle_{\Omega_2}\\ &= v_1^c\boldsymbol{\sigma}_1^c\cdot\langle \boldsymbol{E}\rangle_{\Omega_1} + v_2^c\boldsymbol{\sigma}_2^c\cdot\langle \boldsymbol{E}\rangle_{\Omega_2}\\ &= \boldsymbol{\sigma}_1^c\cdot(\langle \boldsymbol{E}\rangle_{\Omega} - v_2^c\langle \boldsymbol{E}\rangle_{\Omega_2}) + v_2^c\boldsymbol{\sigma}_2^c\cdot\langle \boldsymbol{E}\rangle_{\Omega_2}\\ &= \underbrace{\left(\boldsymbol{\sigma}_1^c + v_2^c(\boldsymbol{\sigma}_2^c - \boldsymbol{\sigma}_1^c)\cdot\boldsymbol{C}_{E,2}\right)}_{\boldsymbol{\sigma}^{c,*}}\cdot\langle \boldsymbol{E}\rangle_{\Omega},\end{aligned} \tag{30}$$

where

$$\underbrace{\left(\frac{1}{v_2^c}(\boldsymbol{\sigma}_2^c - \boldsymbol{\sigma}_1^c)^{-1}\cdot(\boldsymbol{\sigma}^{c,*} - \boldsymbol{\sigma}_1^c)\right)}_{\overset{\text{def}}{=}\boldsymbol{C}_{E,2}}\cdot\langle \boldsymbol{E}\rangle_{\Omega} = \langle \boldsymbol{E}\rangle_{\Omega_2}. \tag{31}$$

$\boldsymbol{C}_{E,2}$ is known as the electric field concentration tensor. Thus, the product of $\boldsymbol{C}_{E,2}$ with $\langle \boldsymbol{E}\rangle_{\Omega}$ yields $\langle \boldsymbol{E}\rangle_{\Omega_2}$. *It is important to realize that once either $\boldsymbol{C}_{E,2}$ or $\boldsymbol{\sigma}^{c,*}$ are known, the other can be computed.* In order to determine the concentration tensor for phase 1, we have from Eq. (27)

$$\langle \boldsymbol{E}\rangle_{\Omega_1} = \frac{\langle \boldsymbol{E}\rangle_{\Omega} - v_2^c\langle \boldsymbol{E}\rangle_{\Omega_2}}{v_1^c} = \frac{(\mathbf{1} - v_2^c\boldsymbol{C}_{E,2})\cdot\langle \boldsymbol{E}\rangle_{\Omega}}{v_1^c} \overset{\text{def}}{=} \boldsymbol{C}_{E,1}\cdot\langle \boldsymbol{E}\rangle_{\Omega}, \tag{32}$$

where

$$\boldsymbol{C}_{E,1} = \frac{1}{v_1^c}(\mathbf{1} - v_2^c\boldsymbol{C}_{E,2}) = \frac{\mathbf{1} - v_2^c\boldsymbol{C}_{E,2}}{1 - v_2^c}. \tag{33}$$

Note that Eq. (33) implies

$$\underbrace{v_1^c\boldsymbol{C}_{E,1}}_{\text{phase}-1\text{ contribution}} + \underbrace{v_2^c\boldsymbol{C}_{E,2}}_{\text{phase}-2\text{ contribution}} = \mathbf{1}. \tag{34}$$

Similarly, for the current, we have

$$\langle \boldsymbol{J}\rangle_{\Omega} = \boldsymbol{\sigma}^{c,*}\cdot\langle \boldsymbol{E}\rangle_{\Omega} \Rightarrow \boldsymbol{\sigma}^{c,*-1}\cdot\langle \boldsymbol{J}\rangle_{\Omega} = \boldsymbol{C}_{E,2}^{-1}\cdot\langle \boldsymbol{E}\rangle_{\Omega_2} = \boldsymbol{C}_{E,2}^{-1}\cdot\boldsymbol{\sigma}_2^{-1}\cdot\langle \boldsymbol{J}\rangle_{\Omega_2}. \tag{35}$$

Thus,

$$\underbrace{\boldsymbol{\sigma}_2^c\cdot\boldsymbol{C}_{E,2}\cdot\boldsymbol{\sigma}^{c,*-1}}_{\boldsymbol{C}_{J,2}}\cdot\langle \boldsymbol{J}\rangle_{\Omega} = \langle \boldsymbol{J}\rangle_{\Omega_2}, \tag{36}$$

and

$$\boldsymbol{C}_{J,1}\cdot\langle \boldsymbol{J}\rangle_{\Omega} = \langle \boldsymbol{J}\rangle_{\Omega_1} \tag{37}$$

where

$$\boldsymbol{C}_{J,1} = \frac{\mathbf{1} - v_2^c\boldsymbol{C}_{J,2}}{1 - v_2^c} = \boldsymbol{\sigma}_1^c\cdot\boldsymbol{C}_{E,1}\cdot\boldsymbol{\sigma}^{c,*-1}. \tag{38}$$

We remark that from Eq. (38) implies

$$\underbrace{v_1^c\boldsymbol{C}_{J,1}}_{\text{phase}-1\text{ contribution}} + \underbrace{v_2^c\boldsymbol{C}_{J,2}}_{\text{phase}-2\text{ contribution}} = \mathbf{1}. \tag{39}$$

Summarizing, we have the following results:

- $\boldsymbol{C}_{E,1}\cdot\langle \boldsymbol{E}\rangle_{\Omega} = \langle \boldsymbol{E}\rangle_{\Omega_1}$ where $\boldsymbol{C}_{E,1} = \frac{1}{v_1^c}(\mathbf{1} - v_2^c\boldsymbol{C}_{E,2}) = \frac{\mathbf{1}-v_2^c\boldsymbol{C}_{E,2}}{1-v_2^c}$,
- $\boldsymbol{C}_{E,2}\cdot\langle \boldsymbol{E}\rangle_{\Omega} = \langle \boldsymbol{E}\rangle_{\Omega_2}$ where $\boldsymbol{C}_{E,2} = \frac{1}{v_2^c}(\boldsymbol{\sigma}_2^c - \boldsymbol{\sigma}_1^c)^{-1}\cdot(\boldsymbol{\sigma}^{c,*} - \boldsymbol{\sigma}_1^c)$,
- $\boldsymbol{C}_{J,1}\cdot\langle \boldsymbol{J}\rangle_{\Omega} = \langle \boldsymbol{J}\rangle_{\Omega_1}$ where $\boldsymbol{C}_{J,1} = \frac{\mathbf{1}-v_2^c\boldsymbol{C}_{J,2}}{1-v_2^c} = \boldsymbol{\sigma}_1^c\cdot\boldsymbol{C}_{E,1}\cdot\boldsymbol{\sigma}^{c,*-1}$,
- $\boldsymbol{C}_{J,2}\cdot\langle \boldsymbol{J}\rangle_{\Omega} = \langle \boldsymbol{J}\rangle_{\Omega_2}$ where $\boldsymbol{C}_{J,2} = \boldsymbol{\sigma}_2^c\cdot\boldsymbol{C}_{E,2}\cdot\boldsymbol{\sigma}^{c,*-1}$.

One may write

$$\begin{gathered}\underbrace{v_1^c\boldsymbol{C}_{E,1}}_{\text{phase}-1\text{ contribution}} + \underbrace{v_2^c\boldsymbol{C}_{E,2}}_{\text{phase}-2\text{ contribution}} = \mathbf{1}\\ \underbrace{v_1^c\boldsymbol{C}_{J,1}}_{\text{phase}-1\text{ contribution}} + \underbrace{v_2^c\boldsymbol{C}_{J,2}}_{\text{phase}-2\text{ contribution}} = \mathbf{1}\end{gathered} \tag{40}$$

Frequently, the first term in the above expressions is referred to as "phase-1's" share, while the second term is "phase-2's" share. Thus, the concentration tensor tells you how much of the overall load is carried by the particles and how much by the matrix. This is useful shortly, when we want to compute the Joule heating in the system.

4.5. Macro–micro Joule heating

One of the key quantities of interest here is the amount of heat generated from running a current through a material, denoted H (a rate), which feeds into the general first law of thermodynamics

$$\rho \dot{w} - \boldsymbol{\sigma} : \nabla \dot{\boldsymbol{u}} + \nabla \cdot \boldsymbol{q} = \underbrace{H.}_{Jouleheating\ source} \tag{41}$$

In Eq. (41), ρ is the mass density, w is the stored energy per unit mass, $\boldsymbol{\sigma}$ is Cauchy stress, $\boldsymbol{u}$ is the displacement field, $\boldsymbol{q}$ is heat flux, and $H = a(\boldsymbol{J} \cdot \boldsymbol{E})$, is the rate of electrical energy absorbed due to Joule heating, where $\boldsymbol{J}$ is the current, $\boldsymbol{E}$ is the electric field and $0 \le a \le 1$ is an absorption constant. Our objective in this work is to determine the phase-wise load-shares of the Joule-field, denoted $H = \boldsymbol{J} \cdot \boldsymbol{E}$, carried by the components in the heterogeneous mixture. The Joule heating Material 1 (eventually assuming isotropy)

$$H_1 = \langle \boldsymbol{J} \rangle_{\Omega_1} \cdot \langle \boldsymbol{E} \rangle_{\Omega_1} = \langle \boldsymbol{J} \rangle_{\Omega_1} \cdot \boldsymbol{\sigma}_1^{c,-1} \cdot \langle \boldsymbol{J} \rangle_{\Omega_1} = \frac{\langle \boldsymbol{J} \rangle_{\Omega_1} \cdot \langle \boldsymbol{J} \rangle_{\Omega_1}}{\sigma_1^c} \tag{42}$$

The Joule heating Material 2:

$$H_2 = \langle \boldsymbol{J} \rangle_{\Omega_2} \cdot \langle \boldsymbol{E} \rangle_{\Omega_2} = \langle \boldsymbol{J} \rangle_{\Omega_2} \cdot \boldsymbol{\sigma}_2^{c,-1} \cdot \langle \boldsymbol{J} \rangle_{\Omega_2} = \frac{\langle \boldsymbol{J} \rangle_{\Omega_2} \cdot \langle \boldsymbol{J} \rangle_{\Omega_2}}{\sigma_2^c} \tag{43}$$

These can be rewritten in terms of macroscale quantities: $\langle \boldsymbol{J} \rangle_{\Omega}$ and $\langle \boldsymbol{E} \rangle_{\Omega}$:

$$H_1 = (\boldsymbol{C}_{J,1} \cdot \langle \boldsymbol{J} \rangle_{\Omega_1}) \cdot (\boldsymbol{C}_{E,1} \cdot \langle \boldsymbol{E} \rangle_{\Omega_1}) = C_{J,1} C_{E,1} \langle \boldsymbol{J} \rangle_{\Omega} \cdot \langle \boldsymbol{E} \rangle_{\Omega} \tag{44}$$

and

$$H_2 = (\boldsymbol{C}_{J,2} \cdot \langle \boldsymbol{J} \rangle_{\Omega_2}) \cdot (\boldsymbol{C}_{E,2} \cdot \langle \boldsymbol{E} \rangle_{\Omega_2}) = C_{J,2} C_{E,2} \langle \boldsymbol{J} \rangle_{\Omega} \cdot \langle \boldsymbol{E} \rangle_{\Omega}. \tag{45}$$

If the overall property is isotropic (assumed above), and each of the constituents is isotropic (for example a microstructure comprised of a continuous isotropic binder embedded with randomly distributed isotropic particles), then we have the following, $\boldsymbol{C}_{E,i} = C_{E,i}\mathbf{1}$ where, for a two-phase material

$$C_{E,1} = \frac{1}{1 - v_2^c} \frac{\sigma_2^c - \sigma^{c,*}}{\sigma_2^c - \sigma_1^c} \text{ and } C_{E,2} = \frac{1}{v_2^c} \frac{\sigma^{c,*} - \sigma_1^c}{\sigma_2^c - \sigma_1^c}, \tag{46}$$

and $\boldsymbol{C}_{J,i} = C_{J,i}\mathbf{1}$, leading to

$$C_{J,1} = \frac{\sigma_1^c}{\sigma^{c,*}(1 - v_2^c)} \left(\frac{\sigma_2^c - \sigma^{c,*}}{\sigma_2^c - \sigma_1^c} \right) \text{ and } C_{J,2} = \frac{\sigma_2^c}{\sigma^{c,*} v_2^c} \left(\frac{\sigma^{c,*} - \sigma_1^c}{\sigma_2^c - \sigma_1^c} \right). \tag{47}$$

The product of the concentration functions take the following form:

$$C_{E,1} C_{J,1} = \frac{\sigma_1^c}{\sigma^{c,*}} \left(\frac{1}{(1 - v_2^c)} \left(\frac{\sigma_2^c - \sigma^{c,*}}{\sigma_2^c - \sigma_1^c} \right) \right)^2 \tag{48}$$

and

$$C_{E,2} C_{J,2} = \frac{\sigma_2^c}{\sigma^{c,*}} \left(\frac{1}{v_2^c} \left(\frac{\sigma^{c,*} - \sigma_1^c}{\sigma_2^c - \sigma_1^c} \right) \right)^2. \tag{49}$$

Because the concentration functions depend on $\sigma^{c,*}$, which in turn depends on σ_1^c, σ_2^c, v_2^c, and the microstructure, we need to employ estimates for $\sigma^{c,*}$.

Remark. Explicitly, for the product of concentration functions, embedding the effective property estimates, we have

$$C_{E,1} C_{J,1} \approx \frac{\sigma_1^c}{(\phi^c \sigma^{c,*,+} + (1 - \phi^c)\sigma^{c,*,-})} \left(\frac{1}{(1 - v_2^c)} \left(\frac{\sigma_2^c - (\phi^c \sigma^{c,*,+} + (1 - \phi^c)\sigma^{c,*,-})}{\sigma_2^c - \sigma_1^c} \right) \right)^2 \tag{50}$$

and

$$C_{E,2} C_{J,2} \approx \frac{\sigma_2^c}{(\phi^c \sigma^{c,*,+} + (1 - \phi^c)\sigma^{c,*,-})} \left(\frac{1}{v_2^c} \left(\frac{(\phi^c \sigma^{c,*,+} + (1 - \phi^c)\sigma^{c,*,-}) - \sigma_1^c}{\sigma_2^c - \sigma_1^c} \right) \right)^2. \tag{51}$$

5. Macroscale thermal properties and macro–micro fields

The effective thermal conductivity is given by $\mathbb{K}^*$ using convex combinations of the Hashin–Shtrikman bounds as approximations for the effective moduli $\mathbb{K}^* \approx \phi^K \mathbb{K}^{*+} + (1-\phi^K)\mathbb{K}^{*-}$, where $0 \leq \phi^K \leq 1$. The effective thermal conductivity estimates are, for two isotropic materials with an overall isotropic response we utilize the following estimates.

$$\underbrace{\mathbb{K}_1 + \frac{v_2^K}{\frac{1}{\mathbb{K}_2-\mathbb{K}_1} + \frac{1-v_2^K}{3\mathbb{K}_1}}}_{\mathbb{K}^{*,-}} \leq \mathbb{K}^* \leq \underbrace{\mathbb{K}_2 + \frac{1-v_2^K}{\frac{1}{\mathbb{K}_1-\mathbb{K}_2} + \frac{v_2^K}{3\mathbb{K}_2}}}_{\mathbb{K}^{*,+}}, \tag{52}$$

where the conductivity of phase 2 (with volume fraction v_2^K) is larger than phase 1 ($\mathbb{K}_2 \geq \mathbb{K}_1$). Usually, v_2^K corresponds to the particle material, although there can be applications where the matrix is more conductive that the particles. In that case, v_2^K would correspond to the matrix material. To obtain the concentration of the thermal fields in each phase, the exact procedure holds with $\nabla\theta$ replacing $\boldsymbol{E}$, $\boldsymbol{q}$ replacing $\boldsymbol{J}$, $\mathbb{K}$ replacing $\boldsymbol{\sigma}^c$, v_1^K replacing v_1^c and v_2^K replacing v_2^c. For thermal properties following concentration tensors:

- $\boldsymbol{C}_{\theta,2} \cdot \langle\nabla\theta\rangle_\Omega = \langle\nabla\theta\rangle_{\Omega_2}$ where $\boldsymbol{C}_{\theta,2} = \frac{1}{v_2^K}(\mathbb{K}_2 - \mathbb{K}_1)^{-1} \cdot (\mathbb{K}^* - \mathbb{K}_1)$
- $\boldsymbol{C}_{\theta,1} \cdot \langle\nabla\theta\rangle_\Omega = \langle\nabla\theta\rangle_{\Omega_1}$ where $\boldsymbol{C}_{\theta,1} = \frac{1}{v_1^K}(\boldsymbol{1} - v_2^K \boldsymbol{C}_{\theta,2}) = \frac{\boldsymbol{1} - v_2^K \boldsymbol{C}_{\theta,2}}{1-v_2^K}$
- $\boldsymbol{C}_{q,2} \cdot \langle\boldsymbol{q}\rangle_\Omega = \langle\boldsymbol{q}\rangle_{\Omega_2}$ where $\boldsymbol{C}_{q,2} = \mathbb{K}_2 \cdot \boldsymbol{C}_{\theta,2} \cdot \mathbb{K}^{*-1}$
- $\boldsymbol{C}_{q,1} \cdot \langle\boldsymbol{q}\rangle_\Omega = \langle\boldsymbol{q}\rangle_{\Omega_1}$ where $\boldsymbol{C}_{q,1} = \frac{\boldsymbol{1} - v_2^K \boldsymbol{C}_{q,2}}{1-v_2^K}$

One may write

$$\begin{aligned} &\underbrace{v_1^K \boldsymbol{C}_{\theta,1}}_{\text{phase}-1\text{ contribution}} + \underbrace{v_2^K \boldsymbol{C}_{\theta,2}}_{\text{phase}-2\text{ contribution}} = \boldsymbol{1} \\ &\underbrace{v_1^K \boldsymbol{C}_{q,1}}_{\text{phase}-1\text{ contribution}} + \underbrace{v_2^K \boldsymbol{C}_{q,2}}_{\text{phase}-2\text{ contribution}} = \boldsymbol{1}. \end{aligned} \tag{53}$$

As before, the first term in the above expressions is referred to as "phase-1's" share, while the second term is "phase-2's" share. Thus, the concentration tensor tells you how much of the overall load is carried by the particles and how much by the matrix.

Remarks. For the thermal fields, we assume that the thermal gradient concentration functions,

$$C_{\theta,1}\langle\nabla\theta\rangle_\Omega = \langle\nabla\theta\rangle_{\Omega_1} \text{ and } C_{\theta,2}\langle\nabla\theta\rangle_\Omega = \langle\nabla\theta\rangle_{\Omega_2} \tag{54}$$

hold for the state variable θ as well, namely:

$$C_{\theta,1}\langle\theta\rangle_\Omega \approx \langle\theta\rangle_{\Omega_1} \text{ and } C_{\theta,2}\langle\theta\rangle_\Omega \approx \langle\theta\rangle_{\Omega_2}. \tag{55}$$

The implication of this statement is as follows

$$\langle\theta\rangle_\Omega = v_1^K\langle\theta\rangle_{\Omega_1} + v_2^K\langle\theta\rangle_{\Omega_2} = v_1^K C_{\theta,1}\langle\theta\rangle_\Omega + v_2^K C_{\theta,2}\langle\theta\rangle_\Omega, \tag{56}$$

which implies the following true statement

$$v_1^K C_{\theta,1}\langle\theta\rangle_\Omega + v_2^K C_{\theta,2}\langle\theta\rangle_\Omega = 1, \tag{57}$$

which helps justify this approximation.

6. Numerical experiments

We consider the two-phase core material comprised of gas hydrates and a binding material.

6.1. Problem setting

The set up for the model problem (Fig. 1), which is in the form of a one-dimensional long cylinder (core sample) with an applied oscillatory current, governed by Eqs. (4)–(7), applied at the top. The Finite Difference grid is one-dimensional (Fig. 1). The following spatio-temporal simulation parameters were used:

- The number of FDTD nodes in the system: N = 200.
- The time-step size: $\Delta t = 0.0001$ s.
- The time limit: 1000s.
- The length of the domain: 1 meter.

The boundary conditions and current density were as follows:

- The temperature at the top: $\theta(z=0)=300$ K.
- The temperature at the bottom: $\theta(z=L)=300$ K.
- The temperature of the surroundings: $\theta^{surr}=300$ K.
- The reference temperature: $\theta^{o}=300$ K.
- The current density: $J_o=100\ \mathrm{amp/m^2}$.
- The current temporal frequency: 10 Hz.

The chosen material parameters were (not intended to represent in-field data):

- The macroscopic pre-exponential attenuation coefficient: $a_o=1\ \mathrm{m}^{-1}$.
- The macroscopic frequency decay dependency: $a_1=0.01\ \mathrm{Hz}^{-1}$.
- The electrical conductivity thermal sensitivity for material 1: $a_{1,2}=1$.
- The electrical conductivity thermal sensitivity for material 2: $a_{2,2}=1$.
- The effective thermal loss parameter: $\beta=1\ \mathrm{W/(m^3-K)}$.
- The baseline value of the electrical conductivity for material 1: $\sigma_{1o}=0.01\ \mathrm{amp-C/Nt-m^2}$.
- The baseline value of the electrical conductivity for material 2: $\sigma_{2o}=0.001\ \mathrm{amp-C/Nt-m^2}$.
- The Joule heating absorption parameter for material: $\alpha_1=0$.
- The heat capacity of material 1: $C_1=1500\ \mathrm{J/kg-K}$,
- The density of material 1: 2600 $\mathrm{kg/m^3}$.
- The thermal conductivity of material 1: 10 W/mK.
- The Joule heating absorption parameter for material: $\alpha_2=1$.
- The heat capacity of material 2: $C_2=2100\ \mathrm{J/kg-K}$.
- The density of material 2: 2000 $\mathrm{kg/m^3}$.
- The thermal conductivity of material 2: 2.2 W/mK.
- The volume fractions: $v_2^c=v_2^K=0.5$.
- The averaging parameter: $\phi^c=\phi^K=0.25$.

6.2. Results

The results are shown in Fig. 5, where the model computes the evolution of the overall (macroscopic) thermal field at each point in the mixture and also the thermal fields in each phase (matrix and particles/hydrates) at each point in the system. In this particular case, relative to the overall mixture, the temperature is higher in the gas hydrates (a rise of approximately 200 K) and relatively lower in the interstitial medium. The arrows (Fig. 5) indicate the instantaneous value of the electrical field at that location. The utility of the model is that it can be rapidly computed and allows analysts to vary parameters quickly, which facilitates the potential use of Machine Learning paradigms for data-model calibration. More sophisticated models require other macro–micro fields and properties such as

- Overall electrical permittivity:

  $$\langle \boldsymbol{D}\rangle_{\Omega}=\boldsymbol{\epsilon}^{*}\cdot\langle \boldsymbol{E}\rangle_{\Omega}, \tag{58}$$

  where $\boldsymbol{\epsilon}^{*}$ is the effective electrical permittivity for the mixture, $\langle \boldsymbol{E}\rangle_{\Omega}$ is the volume averaged electric field, $\langle \boldsymbol{D}\rangle_{\Omega}$ is the volume averaged electric field flux,
- Overall magnetic permeability:

  $$\langle \boldsymbol{B}\rangle_{\Omega}=\boldsymbol{\mu}^{*}\cdot\langle \boldsymbol{H}\rangle_{\Omega}, \tag{59}$$

  where μ^{*} is the effective magnetic permeability for the mixture, $\langle \boldsymbol{H}\rangle_{\Omega}$ is the volume averaged magnetic field, $\langle \boldsymbol{B}\rangle_{\Omega}$ is the volume averaged magnetic field flux.

These are needed for more in depth electromagnetic analyses involving the full set of Maxwell's equations coupled to other field equations, as investigated in Zohdi (2010, 2011, 2012a, 2012b, 2013a, 2013b, 2014a, 2014b), Zohdi and Wriggers (2005, 2008).

7. Summary and conclusions

The past two decades has seen an explosive acceleration in GH research and development. Among the most important developments is the increasing focus of research on gas hydrate-bearing sediments (HBS) rather than crystalline hydrate, the improvements in tools available for sample collection and analysis, the emergence of robust numerical simulation capabilities, and the transition of GH resource assessment from in-place estimates to potential extraction (Boswell et al., 2020). The present

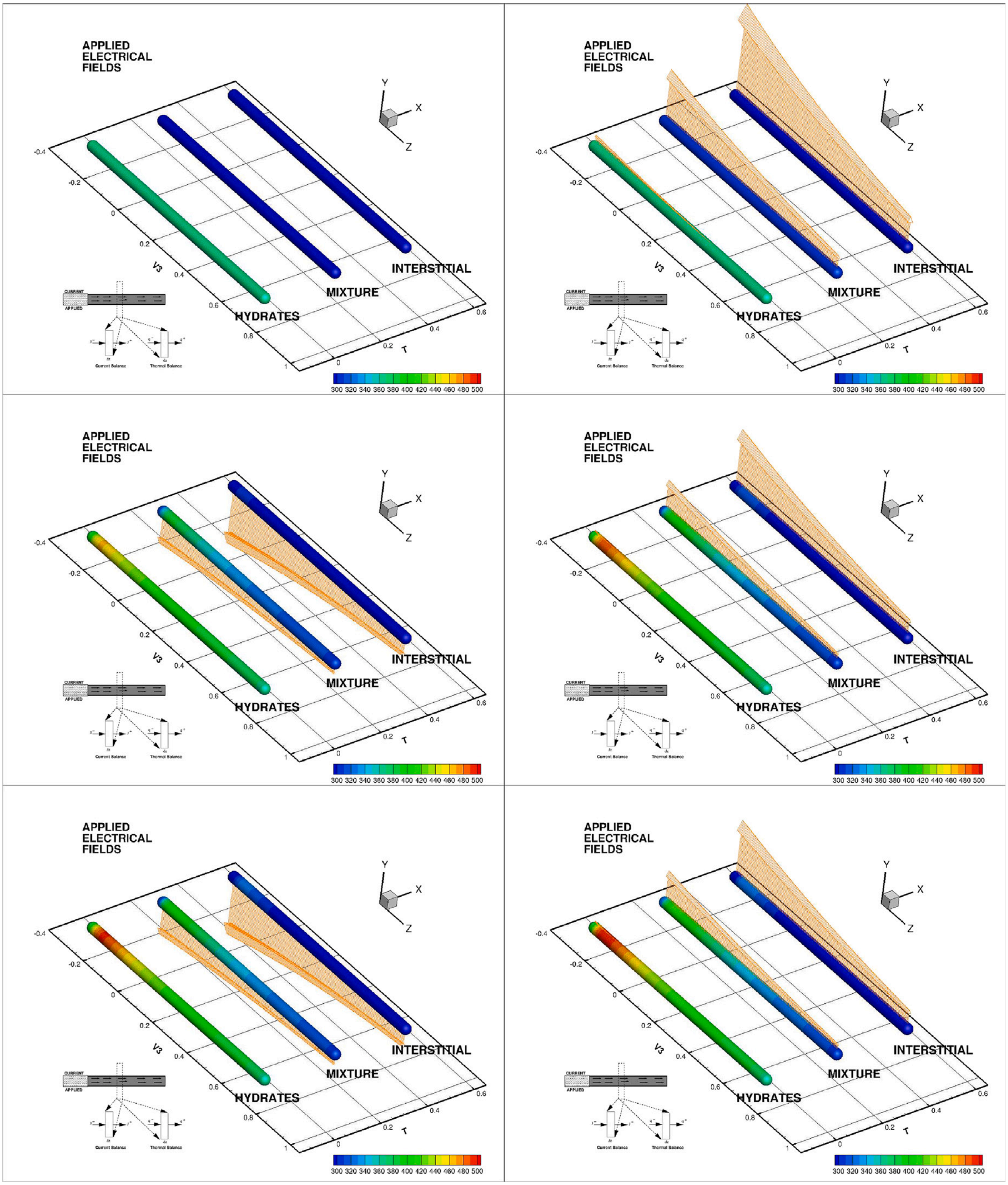

Fig. 5. The evolution of the overall thermal field and the field in each phase in the system. The arrows indicate the instantaneous value of the electrical field at that location.

study works towards making inroads into our understanding of hydrate response under different electrical production scenarios. This work developed a model and rapid simulation strategy for the electrically-driven dissociation (unlocking) of subsurface gas hydrates. As indicated, there are two schools of thought, as to how electrical fields can dissociate gas hydrates: (1) gas hydrates are dissociated (unlocked) by the appropriate intensity and frequency of the electric field or (2) gas hydrates are dissociated by the appropriate level of Joule heating. It is highly likely that it is a combination of both cases. In either case, one must resolve the thermal, electrical and current fields within a heterogeneous medium consisting of encapsulated gas hydrates in a interstitial medium. Accordingly, the objective of this work was to develop a model and simulation strategy to guide the delivery of the appropriate current and electrical field, as well as an appropriate level of Joule heating. Accordingly, the approach developed a coupled system of equations based on electrical-flow and thermal evolution. The model also utilized relations for thermoelectric and frequency-dependent attenuation. Finally, a spatio-temporal Finite-Difference Time Domain (FDTD) discretization was used to efficiently solve the coupled field equations. The model can be computed rapidly and allows analysts to study large parameter ranges quickly, thus enabling the use of Machine Learning paradigms for data-model calibration.

Appendix. Multiphase bounds

In order to make estimates of the overall properties of a mixture of more than two materials mixed together, we illustrate extensions to the Hashin–Shtrikman bounds, for example for electrical conductivity. Accordingly, consider a material with N different phases, σ_1, σ_2 σ_N, where σ_N has the highest conductivity and σ_1, has the lowest. The corresponding volume fractions are v_1, v_2 v_N. There are two possible approximation formulas: (1) The Hill–Reuss–Voigt–Weiner bounds and (2) the multiphase Hashin–Shtrikman bounds.

A.1. The Hill–Reuss–Voigt–Weiner bounds

The HRVW bounds are (Hill, 1952, Reuss, 1929, Voigt, 1889)

$$\left(\sum_{i=1}^{N} \frac{v_i}{\sigma_i}\right)^{-1} \leq \sigma^{c,*} \leq \sum_{i=1}^{N} v_i \sigma_i. \tag{60}$$

A.2. The Hashin–Shtrikman bounds

The HS bounds are

$$\sigma^{c,*,-} = \sigma_1^c + \frac{A_1}{1-\alpha_1 A_1} \leq \sigma^{c,*} \leq \sigma_N^c + \frac{A_N}{1-\alpha_N A_N} \sigma^{c,*,+}, \tag{61}$$

where

$$\alpha_1 = \frac{1}{3\sigma_1^c}, \tag{62}$$

and

$$\alpha_N = \frac{1}{3\sigma_N^c} \tag{63}$$

and

$$A_1 = \sum_{i=2}^{N} \frac{v_i}{(\sigma_i^c - \sigma_1^c)^{-1} + \alpha_1} \tag{64}$$

and

$$A_N = \sum_{i=1}^{N-1} \frac{v_i}{(\sigma_i^c - \sigma_N^c)^{-1} + \alpha_N} \tag{65}$$

For two isotropic materials with an overall isotropic response, this collapses to

$$\underbrace{\sigma_1^c + \frac{v_2}{\frac{1}{\sigma_2^c - \sigma_1^c} + \frac{1-v_2}{3\sigma_1^c}}}_{\sigma^{c,*,-}} \leq \sigma^{c,*} \leq \underbrace{\sigma_2^c + \frac{1-v_2}{\frac{1}{\sigma_1^c - \sigma_2^c} + \frac{v_2}{3\sigma_2^c}}}_{\sigma^{c,*,+}}, \tag{66}$$

where the conductivity of phase 2 (with volume fraction v_2) is larger than phase 1 ($\sigma_2^c \geq \sigma_1^c$). Usually, v_2 corresponds to the particle material, although there can be applications where the matrix is more conductive that the particles. In that case, v_2 corresponds to the matrix material.

References

Aleksandrof, A. A., Dzhuraeva, E. V., & Utenkov, V. F. (2013). Thermal conductivity of sodium chloride aqueous solution. *Thermal Engineering*, *60*(3), 190–194.

Anno, K., Moridis, G. J., & Blasingame, T. A. (2021). JFTS+H: A julia-based parallel simulator for the description of the coupled flow. *Vol. 19*, In *Thermal and geochemical processes in hydrate-bearing geologic media, SPE paper 203953, proceedings, SPE reservoir simulation conference*. http://dx.doi.org/10.2118/203953-MS.

Atkinson, A. B. (2002). A model for the PTX Properties of H_2O-NaCl. (M.S. Thesis), Virginia Polytechnic Institute and State University.

Ballard, A. L. (2002). A non-ideal hydrate solid solution model for a multi-phase equilibria program. (Ph.D. thesis), Colorado School of Mines.

Bear, J. (1972). *Dynamics of fluids in porous media*. New York, London, Amsterdam: American Elsevier Publishing Company.

Bird, R. B., Stewart, W. E., & Lightfoot, E. N. (2007). *Transport phenomena*. New York: John Wiley & Sons, Inc..

Boswell, R., Hancock, S., Yamamoto, K., Collett, T., Pratap, M., & Lee, S. R. (2020). Natural gas hydrates: Status of potential as an energy resource. *Future Energy*, 111–131.

Chung, T. H., Ajlan, M., Lee, L. L., & Starling, K. E. (1988). Generalized multiparameter correlation for nonpolar and polar fluid transport properties. *Industrial and Engineering Chemistry Research*, *27*(4), 671–679. http://dx.doi.org/10.1021/ie00076a024.

Driesner, T. (2007). The system H2O-NaCl. II. Correlation formulae for phase relations in temperature-pressure-composition space from 0 to 1000 °C, 0 to 5000 bar, and 0 to 1 X-NaCl. *Geochimica et Cosmochimica Acta*, *71*, 4880–4901.

Driesner, T., & Heinrich, C. A. (2007). The system H2O-NaCl. I. Correlations for molar volume, enthalpy, and isobaric heat capacity from 0 to 1000 °C, 1 to 5000 bar, and 0 to 1 X-NaCl. *Geochimica et Cosmochimica Acta*, *71*, 4902–4919.

English, N. J., & MacElroy, J. M. D. (2015). *Chemical Engineering Science*, *121*, 133.

Ghosh, S. (2011). *Micromechanical analysis and multi-scale modeling using the voronoi cell finite element method*. CRC Press/Taylor & Francis.

Ghosh, S., & Dimiduk, D. (2011). *Computational methods for microstructure-property relations*. NY: Springer.

Hashin, Z. (1983). Analysis of composite materials: a survey. *ASME Journal of Applied Mechanics*, *50*, 481–505.

Hashin, Z., & Shtrikman, S. (1962a). On some variational principles in anisotropic and nonhomogeneous elasticity. *Journal of the Mechanics and Physics of Solids*, *10*, 335–342.

Hashin, Z., & Shtrikman, S. (1962b). A variational approach to the theory of effective magnetic permeability of multiphase materials. *Journal of Applied Physics*, *33*(10), 3125–3131.

Hashin, Z., & Shtrikman, S. (1963). A variational approach to the theory of the elastic behaviour of multiphase materials. *Journal of the Mechanics and Physics of Solids*, *11*, 127–140.

Hass, J. L. (1976). Physical properties of the coexisting phases and thermochemical properties of the H_2O component in boiling NACl solutions. *Bulletin*, *1421A*.

Hill, R. (1952). The elastic behaviour of a crystalline aggregate. *Proceedings of the Physical Society of London A*, *65*, 349–354.

International Association for the Properties of Water and Steam (IAPWS) (1997). *Release on the IAPWS industrial formulation 1997 for the thermodynamic properties of water and steam*. Erlangen, Germany.

International Association for the Properties of Water and Steam (IAPWS) (2007). *Revised release on the IAPWS industrial formulation 1997 for the thermodynamic properties of water and steam*. Lucerne, Switzerland.

International Association for the Properties of Water and Steam (IAPWS) (2008). *Release on the IAPWS formulation 2008 for the viscosity of ordinary water substance*. Berlin, Germany.

International Association for the Properties of Water and Steam (IAPWS) (2009). *Revised release on the equation of state 2006 for H2O Ice Ih*. Doorwerth, The Netherlands.

International Association for the Properties of Water and Steam (IAPWS) (2011a). *Release on the IAPWS formulation 2011 for the thermal conductivity of ordinary water substance*. Plzeň, Czech Republic.

International Association for the Properties of Water and Steam (IAPWS) (2011b). *Revised release on the pressure along the melting and sublimation curves of ordinary water substance*. Plzeň, Czech Republic.

International Association for the Properties of Water and Steam (IAPWS) (2012). *Guideline on a low-temperature extension of the IAPWS-95 formulation for water vapor*. Boulder, Colorado, USA.

International Formulation Committee (1967). *A formulation of the thermodynamic properties of ordinary water substance*. Düsseldorf, Germany: IFC Secretariat.

Jikov, V. V., Kozlov, S. M., & Olenik, O. A. (1994). *Homogenization of differential operators and integral functionals*. Springer-Verlag.

Kachanov, L. M. (1986). *Introduction to continuum damage mechanics*. Dordricht: Martinus Nijoff.

Kachanov, M. (1993). Elastic solids with many cracks and related problems. *Vol. 30*, In *Advance applied mechanics* (p. 259). New York: Academic Press.

Kachanov, M., & Sevostianov, I. (2005). On the quantitative characterization of microstructures and effective properties. *International Journal of Solids and Structures*, *42*, 309–336.

Kachanov, M., Tsukrov, I., & Shafiro, B. (1994). Effective moduli of solids with cavities of various shapes. *Applied Mechanics Reviews*, *47*, S151–S174.

Kastner, M., Myers, M., Koh, C. A., Moridis, G., Johnson, J. E., & Thurmond, J. (2022). Energy transition and climate mitigation require increased effort on methane hydrate research. *Energy & Fuels*, *36*, 2923–2926. http://dx.doi.org/10.1021/acs.energyfuels.2c00338.

Kim, H. C., Bishnoi, P. R., Heideman, R. A., & Rizvi, S. S. H. (1987). *Chemical Engineering Science*, *42*, 1645–1653.

Klauda, J. B., & Sandler, S. I. (2005). Global distribution of methane hydrate in ocean sediment. *Energy & Fuels*, *19*(469).

Klinkenberg, L. J. The permeability of porous media to liquids and gases. *Vol. 200*, In *API drilling and production practice* (p. 213).

Kröner, E. (1972). *CISM lecture notes*: *Vol. 92*, *Statistical continuum mechanics*. Springer-Verlag.

Makogon, Y. F. (1997). *Hydrates of hydrocarbons*. Tulsa, OK: Penn Well Publishing Co.

Mao, S., & Duan, Z. (2009). The viscosity of aqueous Alkali-Chloride solutions up to 623 K, 1000 bar and high ionic strength. *International Journal of Thermophysics*, *30*, 1510–1523.

Maxwell, J. C. (1867). On the dynamical theory of gases. *Philosophical Transactions of the Royal Society of London*, *157*(49).

Maxwell, J. C. (1873). *A treatise on electricity and magnetism* (3rd ed.). Oxford: Clarendon Press.

Milkov, A. V. (2004). Global estimates of hydrate-bound gas in marine sediments: How much is really out there? *Earth Science Reviews*, *66*(3), 183.

Millington, R. J., & Quirk, J. P. (1961). Permeability of porous solids. *Transactions of the Faraday Society*, *57*, 1200–1207.

Moridis, G. J. (2014). User, manual for the HYDRATE v1.5 option of tough+ v1.5: A code for the simulation of system behavior in hydrate-bearing geologic media. *Lawrence berkeley national laboratory report LBNL-6871E*.

Moridis, G. J., Collett, T. S., Boswell, R., Kurihara, M., Reagan, M. T., Koh, C., et al. (2009). Toward production from gas hydrates: Current status, assessment of resources, and simulation-based evaluation of technology and potential. *SPE Reservoir Evaluation & Engineering*, *12*(5), 745–771. http://dx.doi.org/10.2118/114163-PA.

Moridis, G. J., Collett, T. S., Pooladi-Darvish, M., Hancock, S., Santamarina, C., Boswell, R., et al. (2011). Uncertainties and issues facing gas production from gas hydrate deposits. *SPE Reservoir Evaluation & Engineering*, *14*(1), 76–112. http://dx.doi.org/10.2118/131792-PA.

Moridis, G. J., & Pruess, K. (2014). User manual of the tough+v1.5 core code: A general purpose simulator of non-isothermal flow and transport through porous and fractured media. *Lawrence berkeley national laboratory report LBNL-6869E*.

Mura, T. (1993). *Micromechanics of defects in solids* (2nd ed.). Kluwer Academic Publishers.

Nemat-Nasser, S., & Hori, M. (1999). *Micromechanics: Overall properties of heterogeneous solids* (2nd ed.). Amsterdam: Elsevier.

Peng, D. Y., & Robinson, D. B. (1976). A new two-constant equation of state. *Industrial & Engineering Chemistry Fundamentals*, *15*, 59–64.

Pruess, K., Oldenburg, C., & Moridis, G. (1999). *TOUGH2 user guide, version 2.0, report LBNL-43134*, Berkeley, Calif: Lawrence Berkeley National Laboratory.

Pruess, K., Oldenburg, C., & Moridis, G. (2012). *TOUGH2 user guide, version 2.1, report LBNL-43134*, Berkeley, Calif: Lawrence Berkeley National Laboratory.

Rayleigh, J. W. (1892). On the influence of obstacles arranged in rectangular order upon properties of a medium. *Philosophical Magazine*, *32*, 481–491.

Reuss, A. (1929). Berechnung der Fliessgrenze von Mischkristallen auf Grund der Plastizitätsbedingung für Einkristalle. *Zeitschrift fur Angewandte Mathematik und Mechanik*, *9*, 49–58.

Rojey, A. (1997). Process and system using an electromagnetic wave to prevent the formation of hydrates. U.S. patent 5, 652, 178, 29.

Sevostianov, I., Gorbatikh, L., & Kachanov, M. (2001). Recovery of information of porous / microcracked materials from the effective elastic/conductive properties. *Materials Science and Engineering. A*, *318*, 1–14.

Sloan, E. D., & Koh, C. (2008). *Clathrate hydrates of natural gases* (3rd ed.). Boca Raton, FL: Taylor and Francis, Inc..

Torquato, S. (2002b). *Random heterogeneous materials: microstructure & macroscopic properties*. New York: Springer-Verlag.

Voigt, W. (1889). Über die Beziehung zwischen den beiden Elastizitätskonstanten isotroper Körper. *Wied. Ann*, *38*, 573–587.

Wiener, O. (1910). Zur theorie der refraktionskonstanten. In *Math.-phys Klasses, Band 62*, *Berichte über die verhandlungen der königlich-sächsischen gesellschaft der wissenshaften zu leipzig* (pp. 256–277).

Zohdi, T. I. (2010). Simulation of coupled microscale multiphysical-fields in particulate-doped dielectrics with staggered adaptive FDTD. *Computer Methods in Applied Mechanics and Engineering*, *199*, 79–101.

Zohdi, T. I. (2011). Joule heating field phase-amplification in particulate-doped dielectrics. *The International Journal of Engineering Science*, *49*, 30–40.

Zohdi, T. I. (2012a). Electromagnetic properties of multiphase dielectrics. In *A primer on modeling, theory and computation*. https://rd.springer.com/book/10.1007/978-3-642-28427-4.

Zohdi, T. I. (2012b). Estimation of electrical-heating load-shares for sintering of powder mixtures. *Proceedings of the Royal Society*, *468*, 2174–2190.

Zohdi, T. I. (2013a). Electromagnetically-induced vibration in particulate-doped materials. *ASME Journal of Vibration and Acoustics*.

Zohdi, T. I. (2013b). Modeling electrical power absorption and thermally-induced biological tissue damage. *Biomechanics and Modeling in Mechanobiology*, http://dx.doi.org/10.1007/s10237-013-0489-9.

Zohdi, T. I. (2014a). A direct particle-based computational framework for electrically-enhanced thermo-mechanical sintering of powdered materials. *Mathematics and Mechanics of Solids*, 1–21. http://dx.doi.org/10.1007/s11831-013-9092-6.

Zohdi, T. I. (2014b). On cross-correlation between thermal gradients and electric fields. *The International Journal of Engineering Science*, *74*, 143–150.

Zohdi, T. I., Monteiro, P. J. M., & Lamour, V. (2002). Extraction of elastic moduli from granular compacts. *The International Journal of Fracture/Letters in Micromechanics*, *115*, L49–L54.

Zohdi, T. I., & Wriggers, P. (2005, 2008). *Introduction to computational micromechanics*. Springer-Verlag, Second Reprinting.